ORIGINAL RESEARCH

# Osteogenic cell differentiation on H-terminated and O-terminated nanocrystalline diamond films

Jana Liskova[1]
Oleg Babchenko[2]
Marian Varga[2]
Alexander Kromka[2]
Daniel Hadraba[1]
Zdenek Svindrych[1]
Zuzana Burdikova[1]
Lucie Bacakova[1]

[1]Institute of Physiology, Academy of Sciences of the Czech Republic, Prague, Czech Republic; [2]Institute of Physics, Academy of Sciences of the Czech Republic, Prague, Czech Republic

**Abstract:** Nanocrystalline diamond (NCD) films are promising materials for bone implant coatings because of their biocompatibility, chemical resistance, and mechanical hardness. Moreover, NCD wettability can be tailored by grafting specific atoms. The NCD films used in this study were grown on silicon substrates by microwave plasma-enhanced chemical vapor deposition and grafted by hydrogen atoms (H-termination) or oxygen atoms (O-termination). Human osteoblast-like Saos-2 cells were used for biological studies on H-terminated and O-terminated NCD films. The adhesion, growth, and subsequent differentiation of the osteoblasts on NCD films were examined, and the extracellular matrix production and composition were quantified. The osteoblasts that had been cultivated on the O-terminated NCD films exhibited a higher growth rate than those grown on the H-terminated NCD films. The mature collagen fibers were detected in Saos-2 cells on both the H-terminated and O-terminated NCD films; however, the quantity of total collagen in the extracellular matrix was higher on the O-terminated NCD films, as were the amounts of calcium deposition and alkaline phosphatase activity. Nevertheless, the expression of genes for osteogenic markers – type I collagen, alkaline phosphatase, and osteocalcin – was either comparable on the H-terminated and O-terminated films or even lower on the O-terminated films. In conclusion, the higher wettability of the O-terminated NCD films is promising for adhesion and growth of osteoblasts. In addition, the O-terminated surface also seems to support the deposition of extracellular matrix proteins and extracellular matrix mineralization, and this is promising for better osteoconductivity of potential bone implant coatings.

**Keywords:** nanocrystalline diamond film, osteoblast, Saos-2, collagen, SHG

## Introduction

Diamond nanocrystals, either in their isolated form (powder) or in their compact form (fully packed film) are widely considered as a promising material for a wide range of new applications in biology, pharmacology (eg, controlled drug and gene delivery), biomedical diagnostics and analytics (optical imaging, biosensors), and the field of environmental monitoring. Both of these diamond forms show the best biocompatibility and noncytotoxicity of all carbon allotropes.[1,2] To the best of our knowledge, no cytotoxic damage to cells growing on nanodiamond films has been reported. However, films based on carbon nanotubes or on graphene, or films that contain these nanoparticles, have often shown some cytotoxicity for mammalian cells.[3–5]

The diamond surface consists of $sp^3$ hybridized carbon bonds that are chemically and mechanically stable. Nanosized diamond crystals are packed in a compact form as thin films, referred to as nanocrystalline diamond films (NCD), and display a wide range of unique physical and chemical properties, such as mechanical hardness, chemical and thermal resistance, excellent optical transparency, and controllable electrical properties.[2,6,7] The nanostructure and morphology of NCD films can efficiently mimic

Correspondence: Jana Liskova
Institute of Physiology, Academy of Sciences of the Czech Republic, Videnska 1083, Prague 4, CZ-14220, Czech Republic
Tel +42 02 4106 3742
Fax +42 02 4106 2488
Email jana.liskova@biomed.cas.cz

the properties of natural tissues,[8,9] and so they should support cell adhesion, proliferation, and differentiation. In addition, NCD wettability can be tailored by grafting specific atoms and functional chemical groups (eg, oxygen, hydrogen, amine groups) that influence the wettability and surface energy of NCD films.[10] The wettability of the surface affects the adsorption and the final geometry of the proteins, and thus it modulates the behavior of cultivated cells.[11–13] The large area of the nanostructured NCD film surface also contributes to better adsorption of proteins from the environment.[10] NCD films have been shown to coat substrates hermetically,[14] so NCD coatings could prevent the release of harmful ions from metallic implants. NCD films are therefore proposed as multifunctional materials for fundamental studies on the growth and adhesion of osteoblasts on bone implants.

The desired integration of bone implants is dependent on the osteoconductivity of the implant surface. Osteoconduction means that the bone tissue grows on a surface or down into pores or channels of the material.[15] Osteoconduction is achieved by the adhesion, growth, and maturation of osteoblasts, which are manifested by the deposition of newly formed mineralized extracellular matrix (ECM) at the bone–implant interface. The major component of organic ECM in bone tissue is type I collagen. Its fibrous structure ensures appropriate mechanical properties of the bone, which are further enhanced by matrix mineralization. Collagen plays an important role in bone matrix mineralization, particularly by binding the bone sialoprotein, which initiates hydroxyapatite nucleation,[16] and by anchoring other calcium-binding molecules, particularly glycosaminoglycan chondroitin 4-sulfate.[17]

Although type I collagen and the composition and organization of its fibers are some of the most important features, the widely adopted methods of measurement (eg, magnetic resonance imaging, X-ray) usually lack resolution or cause additional errors because of sample preparation (eg, histochemistry). A method that offers both sufficient resolution and the possibility of in vivo measurement is second harmonic generation (SHG) microscopy. This method is suitable for optically nonlinear materials that have strong second order nonlinear susceptibility ($\chi^2$). Then, the resulting magnitude of the SHG signal has quadratic dependence on the number of molecules and the intensity of the incident light.[18] The molecular nature of type I collagen enables SHG emission, and SHG microscopy has therefore become an elementary tool for type I collagen evaluation.

In this study, we intended to evaluate the suitability of NCD films with either high or low wettability as bone implant coatings. We evaluated osteoblast growth and differentiation. We also evaluated ECM production and mineralization on both types of NCD films, because ECM deposition is important for the acceptance of the bone implant in the organism. The quality of the deposited ECM as a marker of the osteoconductivity of the evaluated surfaces was characterized by several approaches, including visualization of mature collagen fibers by using SHG microscopy.

## Materials and methods
### Diamond growth and surface treatment
Diamond thin films were grown on 100 silicon (Si) substrates either of rectangular geometry (10 mm ×10 mm) or of round geometry (63.5 mm in diameter). Before processing, the Si substrates were first ultrasonically cleaned in isopropylalcohol and rinsed in deionized water. Then, they were seeded by applying ultrasonic agitation in a water-based diamond powder suspension (powder from NanoAmando; New Metals and Chemicals Corp. Ltd., Kyobashi, Tokyo, Japan) for 40 minutes. The typical diamond nucleation density after this process is in the range of $10^{11}$ cm$^{-2}$.[19–21]

Diamond films were grown by the pulsed linear antenna microwave chemical vapor deposition process from an $H_2/CH_4/CO_2$ gas mixture.[22,23] The parameters during the deposition process were as follows: 2.5% of $CH_4$ and 10% of $CO_2$ in a hydrogen atmosphere; total gas pressure of 10 Pa; pulsed microwave power of 1.7 kW on both sides of the antenna; and a substrate temperature of 650°C. It should be mentioned that the Si substrates were coated by a diamond film on both sides to minimize any unwanted effect of the Si substrate on the cell cultivation. The diamond film was used to coat the rough side of the Si substrates first and then the mirror-like polished side of the Si substrates afterwards.

After deposition, the diamond-coated Si substrates were postprocessed in two ways. Half of the samples were hydrogenated in a focused microwave chemical vapor deposition system in pure hydrogen plasma for 10 minutes under these conditions: microwave power of 1.5 kW; substrate temperature of about 530°C; and total gas pressure of 3 kPa. The other half of the samples were oxidized in inductively coupled oxygen plasma at a radio-frequency power of 280 W for 3 minutes.

### Raman, scanning electron microscopy (SEM), and atomic force microscopy (AFM)
The deposited diamond films were identified from the Raman spectra acquired by a Renishaw InVia Reflex Raman

spectrometer with an excitation wavelength of 442 nm. The surface morphology was investigated by SEM (e_LiNe workstation; Raith, Dortmund, Germany) in standard configuration. The topography of the diamond films was investigated by AFM (Solver PRO; NT-MDT Co., Moscow, Russia) in tapping mode (Multi75Al-G tip).

## Contact angle measurement

The wetting properties of the as-grown diamond film surfaces, the H-terminated diamond film surfaces, and the O-terminated diamond film surfaces were determined by contact angle measurements at room temperature by using a static method in a material–water droplet system. A water drop 3 µL in volume was dropped on to the investigated diamond surface and the formed drop was captured by a digital charged-couple device camera. The contact angle, used to assess the wetting properties of the surface, was calculated by using the Surface Energy Evaluation System (Masaryk University, Brno, Czech Republic) for the multipoint fitting of the drop profile.

## Cell culture

Square samples 1 $cm^2$ in size or circular samples 63.5 mm in diameter were sterilized with 70% ethanol for 1 hour and were washed three times with a sterile phosphate buffered saline (PBS) solution. The circular samples were placed in 10 cm polystyrene dishes (TPP, Trasadingen, Switzerland) and were used for collagen synthesis determination. The square samples were placed in 24-well polystyrene multidishes (TPP) and were used for all of the other experiments. The samples and controls (polystyrene dishes or microscopic glass) were seeded with human osteoblast-like Saos-2 cells (DSMZ, Braunschweig, Germany). The cells were cultivated in McCoy's 5A medium (Sigma-Aldrich Co., St Louis, MO, USA), supplemented with 10% fetal bovine serum (FBS) (Gibco®; Thermo Fisher Scientific, Waltham, MA, USA) and gentamicin (40 µg/mL) (Novartis International AG, Basel, Switzerland) in a humidified 5% $CO_2$ atmosphere at 37°C. For an evaluation of the cell number, the cells were seeded at a density of 10,000 cells/$cm^2$ and incubated in the growth medium for 3 days. For all of the other experiments, the cells were seeded at a density of 25,000 cells/$cm^2$ and were incubated until they reached 100% confluence (6 days). After reaching confluence, the cell layers were incubated either in the growth medium or in a medium supplemented with 50 µg/mL of ascorbic acid (AA) (Sigma-Aldrich Co.), which was added every day for 14 more days. The medium was exchanged every second or third day during incubation of the confluent cell layers.

## Evaluation of cell number

At time points 24 hours and 72 hours after seeding, the cells were rinsed with PBS, fixed with 70% cold ethanol for 5 minutes, and stained with Texas Red $C_2$–maleimide (20 ng/mL) (Thermo Fisher Scientific) and Hoechst 33258 (5 µg/mL) (Sigma-Aldrich Co.) in PBS for 30 minutes. The cells were then rinsed with PBS and imaged using fluorescence microscopy; from each sample, 20 images from random areas were acquired (two samples in the group), and cell nuclei were counted by using NIS-Elements software (Nikon Instruments, Melville, NY, USA).

## LIVE/DEAD staining

The cell layers from the samples on day 14 after reaching confluence were stained with the LIVE/DEAD® viability/cytotoxicity kit for mammalian cells (Thermo Fisher Scientific) according to the manufacturer's protocol. The cells were then rinsed with PBS and imaged by using fluorescence microscopy.

## Fluorescence microscopy

The fluorescence microscopy images were obtained under an IX 51 epifluorescence microscope equipped with a DP 70 digital camera (both manufactured by Olympus Corp., Tokyo, Japan).

## Immunofluorescence staining

The cells were rinsed with PBS, fixed with 70% cold ethanol, and blocked with 1% bovine serum albumin in PBS for 20 minutes. The primary antibody, mouse monoclonal anti-collagen I antibody, (Abcam, Cambridge, UK) was diluted 1:200 in PBS and applied overnight at 4°C. After being rinsed with PBS, the cells were incubated for 1 hour at room temperature with the secondary antibody (goat antimouse Alexa Fluor 488 conjugate; Thermo Fisher Scientific) that was diluted 1:400 in PBS. The stained cells were then rinsed with PBS and visualized by confocal microscopy (maximum intensity projections of green fluorescence), two-photon excited fluorescence microscopy, and nonlinear microscopy (SHG imaging). The experiments were performed in triplicate and were repeated three times.

## SHG imaging and confocal microscopy

The SHG images were acquired by using Leica TCS SP2 AOBS, a point scanning confocal system (Leica Microsystems GmbH, Wetzlar, Germany). The system is based on the Leica DMIRE2 inverted microscope and is equipped with the mode-locked Ti:Sapphire Chameleon Ultra laser (Coherent

Inc., Santa Clara, CA, USA), which is tunable from 690 nm to 1,040 nm. Because type I collagen fibers generate a strong SHG signal, the infrared short pulse Chameleon laser was adopted to visualize the collagen structures. The laser was tuned to 860 nm, and a half wavelength response was expected in the emission pathway. The SHG signal was detected in the backward nondescanned mode. The signal was collected directly behind the objective (Leica HCX PL APO 63× NA 1.2; water immersion) (Leica Microsystems GmbH) and passed the infrared filter and a 430±10 nm band-pass filter before reaching a photomultiplier tube (magenta channel). To confirm that the detected signal was from SHG and not autofluorescence, the same field of view was excited at 800 nm instead of 860 nm, while the setup (filters) remained unchanged. The images obtained at this setting not only proved the presence of the SHG signal for 860 nm excitation but were also used to define the autofluorescence of the cells (blue channel). Two-photon excited fluorescence microscopy was used to image the immunofluorescence staining of the samples, and the excitation wavelength remained constant (860 nm). Green fluorescence of the samples was detected by using the internal photomultiplier tube detector (490 nm; green channel).

The acquired SHG images (17–26 images from three samples in the group) were analyzed by using ImageJ (US National Institutes of Health, Bethesda, MD, USA). For each image, the threshold was set manually. As the image intensity depends critically on the actual laser power, instrument settings, and focus depth, the intensity-based metrics varied widely among the images. We thus used the image area occupied by collagen (the area of pixels above the threshold) to represent the amount of collagen. To ensure that only mature extracellular collagen was measured, we also thresholded two-photon autofluorescence images and the pixels above the threshold were excluded from the analysis. The results were then expressed as the percentage of the total image area.

The maximum intensity projections of the green immunofluorescence of cells stained for type I collagen were acquired on the Leica TCS SPE upright confocal system (Leica ACS APO 40.0×1.15 oil objective; Leica Microsystems GmbH); the excitation laser was 488 nm and the detector was tuned to 500–599 nm.

## Collagen synthesis
The amount of collagen deposited in the ECM was determined with the Sircol kit (Biocolor Ltd, Carrickfergus, UK). Before the determination, the collagen was recovered from the ECM by acidic pepsin digestion. The cell layers were rinsed with PBS, harvested with a cell scraper in PBS, and centrifuged. The cell pellets were resuspended in a pepsin solution (0.1 mg/mL in 0.5 M AA) and were lysed for 24 hours on ice. The lysates were centrifuged and supernatants were concentrated according to the Sircol kit manufacturer's protocol. The amount of collagen in the samples and the standard curve were then determined using Sirius red dye binding according to the manufacturer's protocol. The results were normalized by the substrate area. The experiments were performed in quadruplicate and were repeated three times.

## Alkaline phosphatase (ALP) activity
The cell layers were twice washed with PBS; then, the substrate solution (0.1 mg/mL p-nitrophenyl phosphate in substrate buffer [50 mM glycine, 1 mM $MgCl_2$, pH 10.5]) (Sigma-Aldrich Co.) was added directly to the cells. The reaction was performed for 5 minutes at room temperature; the substrate solution was then removed and mixed with the same volume of the 1 M NaOH solution. The absorbance (405 nm) of the samples was measured together with the absorbance of the known concentrations of p-nitrophenol diluted in 0.02 M NaOH (9–90 µM) (Sigma-Aldrich Co.). The results were normalized by the substrate area. The resulting values for the concentration of p-nitrophenol were related to the values of the control cells grown on the polystyrene controls (100%). The experiments were performed in triplicate and were repeated three times.

## Calcium deposition
The cell layers were rinsed with PBS, dried, and lysed in 0.5 M HCl for 24 hours at 4°C. The calcium in the cell lysates and standards was directly determined by using the Calcium Colorimetric Assay Kit (Biovision Inc., Milpitas, CA, USA) according to the manufacturer's protocol. The experiments were performed in triplicate and were repeated three times. The results were normalized to the substrate area.

## DNA content
The cell layers were rinsed with PBS and lysed in 0.05% SDS in a Tris–EDTA solution at room temperature by shaking for 30 minutes. The lysates were diluted ten times with Tris–EDTA. The total DNA content in the lysates and the standard curve were determined by using the Quant-iT™ PicoGreen® dsDNA Kit (Thermo Fisher Scientific) according to the manufacturer's protocol. The experiments were performed in triplicate and were repeated three times. The results were normalized to the substrate area.

## Real-time polymerase chain reaction (PCR)

On day 14 postconfluence, the total RNA was extracted from the cell layers by using RNAzol (Molecular Research Center, Cincinnati, OH, USA) according to the manufacturer's protocol. Reverse transcription was performed by using oligo-dT primers and the ProtoScript M-MuLV First Strand cDNA Synthesis Kit (New England Biolabs, Ipswich, MA, USA) according to the manufacturer's protocol. The real-time PCR reactions were performed by using FastStart Universal SYBR Green Master Mix (Hoffman-La Roche Ltd., Basel, Switzerland) on the iQ5 Multicolor Real-Time PCR Detection System (Bio-Rad Laboratories, Inc., Hercules, CA, USA). The real-time PCR parameters were as follows: 40 cycles; 95°C for 10 seconds; and 60°C for 1 minute. The reactions were carried out in duplicate. The real-time PCR data were analyzed in Bio-Rad iQ software (Bio-Rad Laboratories, Inc.) and CFX Manager software by using the $\Delta\Delta C_T$ method and by including the efficiencies of particular primer pairs (Table 1) in order to increase the accuracy of the results. The expression levels of osteoblast marker genes were normalized to the expression of the glyceraldehyde 3-phosphate dehydrogenase gene and were related to the expression levels of the cells on a polystyrene dish harvested on day 1 postconfluence. The experiments were performed in duplicate and were repeated three times. The statistical analysis was performed on $\Delta\Delta C_T$ values.

## Statistical analysis

The quantitative results were presented as the mean ± standard deviation (SD). The statistical analyses were performed by using SigmaStat (Systat Software, San Jose, CA, USA). Multiple comparison procedures were carried out by analysis of variance (ANOVA), or in cases in which the data normality test failed, by the Kruskal–Wallis test. All pairwise multiple comparisons were counted by the Student–Newman–Keuls method. A value of $P \leq 0.05$ was considered significant.

# Results

## Preparation and analysis of NCD films

Figure 1 shows deposited diamond films on both sides of the 10 mm ×10 mm Si substrates in three types of images: the Raman spectra; the top view SEM images; and the AFM images. The Raman spectra (Figure 1A) of the samples measured by the 442 nm ultraviolet excitation wavelength are dominated by sharp peaks centered at a frequency of 1,332 cm⁻¹ (D-peak) of the Raman shift assigned to the diamond phase (ie, sp³ hybridized carbon bonds). The broad band centered in the range of 1,530–1,590 cm⁻¹ (G-band) is attributed to the graphitic sp² hybridized carbon phases. In addition to the D-peak and G-band, two bands can be resolved: the broad band centered at 1,350 cm⁻¹ is attributed to disordered carbon bonds (D-band); and the negligible band localized at approximately 1,150 cm⁻¹ is often assigned to transpolyacetylene fragments and generally represents a signature of the nanocrystalline nature of the diamond film.[24–26]

The surface morphology and the grain size of deposited diamond films are shown in Figure 1B. It was found that the deposited diamond film is homogeneous and void-free, and was composed from densely packed and randomly oriented grains with multiple cracking. The estimated size of the individual grains is up to 300 nm, as was found from the SEM image. The surface of the diamond film deposited on the back side of the Si (on the rough side) reveals some smaller features. These are most probably because of the secondary seeding effect, which happened because of the front side deposition.

The surface topographies of films measured by AFM are shown in Figure 1C. The AFM images reveal uniform and homogeneous coverage of the Si substrate with the diamond film. The scanned area was 10 µm ×10 µm for both AFM images. The calculated root mean square roughness was approximately 18±2 nm for the diamond film deposited on the smooth side of the Si substrate. For the rough side, the AFM measurement was strongly influenced by the primary substrate roughness (hundreds of nm). In this

**Table 1** Real-time PCR primers used in the study

| Gene | Primer sequences (5′-3′) | Product length (base pairs) | Efficiency |
|---|---|---|---|
| Type I collagen[64] | CAGCCGCTTCACCTACAGC TTTTGTATTCAATCACTGTCTTGCC | 83 | 92.5% |
| ALP[64] | GACCCTTGACCCCACAAT GCTGCTACTGCATGTCCCCT | 68 | 90.7% |
| Osteocalcin[64] | GAAGCCCAGCGGTGCA CACTACCTCGCTGCCCTCC | 70 | 104% |
| GAPDH[65] | TGCACCACCAACTGCTTAGC GGCATGGACTGTGGTCATGAG | 87 | 93.3% |

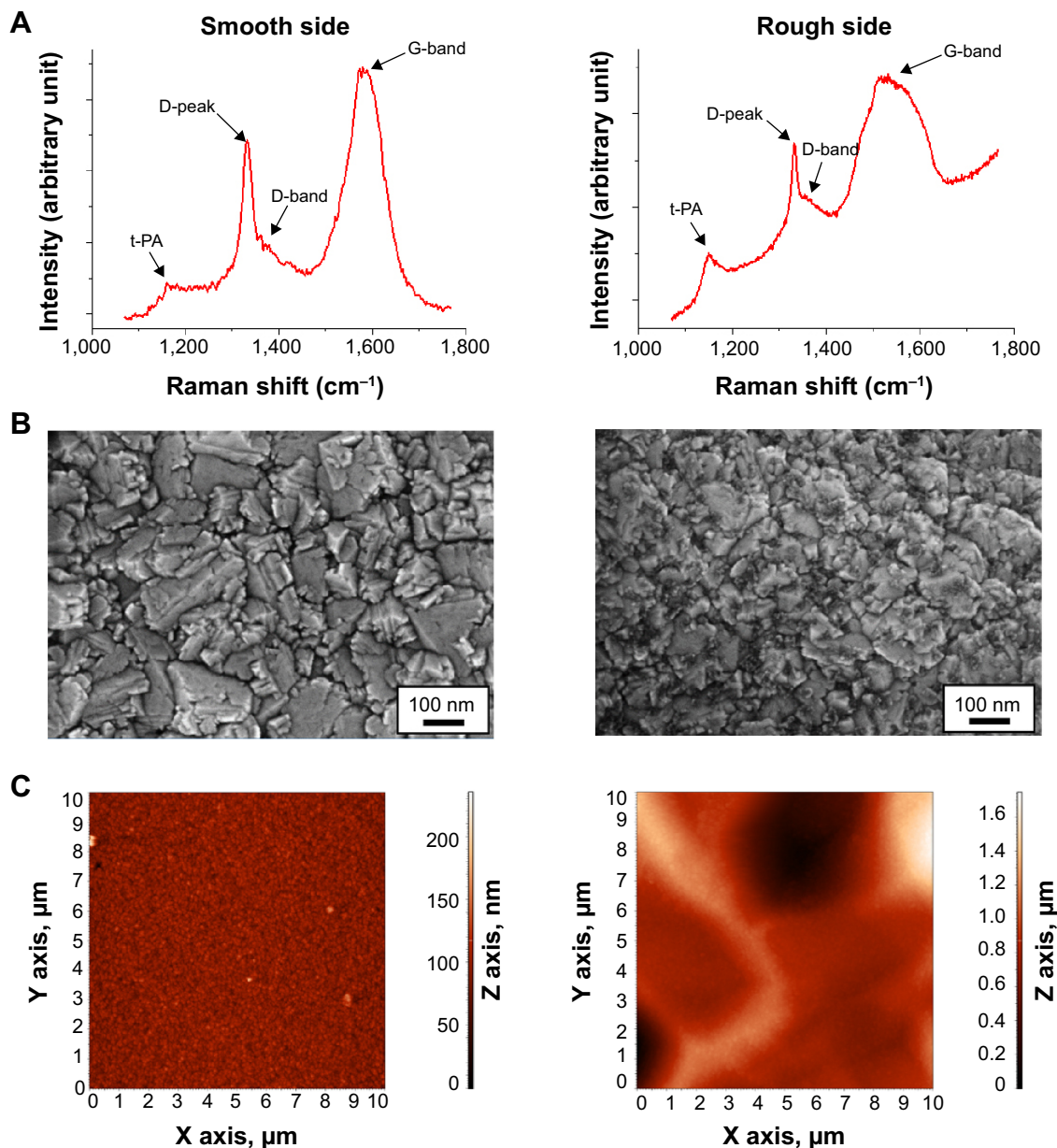**Abbreviations:** PCR, polymerase chain reaction; ALP, alkaline phosphatase; GAPDH, glyceraldehyde 3-phosphate dehydrogenase.

**Figure 1** Characterization of the deposited diamond film.
**Notes:** Raman spectra (**A**); SEM images (**B**); and AFM images (**C**) of the deposited diamond film on the smooth side (left column) and on the rough side (right column) of the silicon substrate.
**Abbreviations:** SEM, scanning electron microscopy; AFM, atomic force microscopy.

sense, the sample surface can be labeled as a hierarchically structured surface in which the diamond layer represents the nanoscale roughness and the rough Si substrate represents the microroughness.[27]

The water contact angle measurements are shown in Figure 2 and summarize the wetting properties of the three types of diamond films: as-grown; H-terminated; and O-terminated. The as-grown sample revealed hydrophobic properties with a contact angle of about 65°. After hydrogen plasma treatment, the diamond film (Diamond H) exhibited stronger hydrophobic properties (contact angle about 100°).

Finally, the oxidized diamond (Diamond O) surface revealed unambiguously hydrophilic properties with a contact angle value lower than 10°. The roughness of the H-terminated and that of O-terminated NCD films were equal, and thus roughness did not influence the wettability of the surface. The same surface roughness for O-termination and for H-termination can be assigned only to an atomic change of the dangling bonds by oxygen and hydrogen. We assume that some minimal damage to the diamond surface on an atomic scale (1–2 nm) can occur. However, in our case, it was below the resolution limit of the AFM measurements
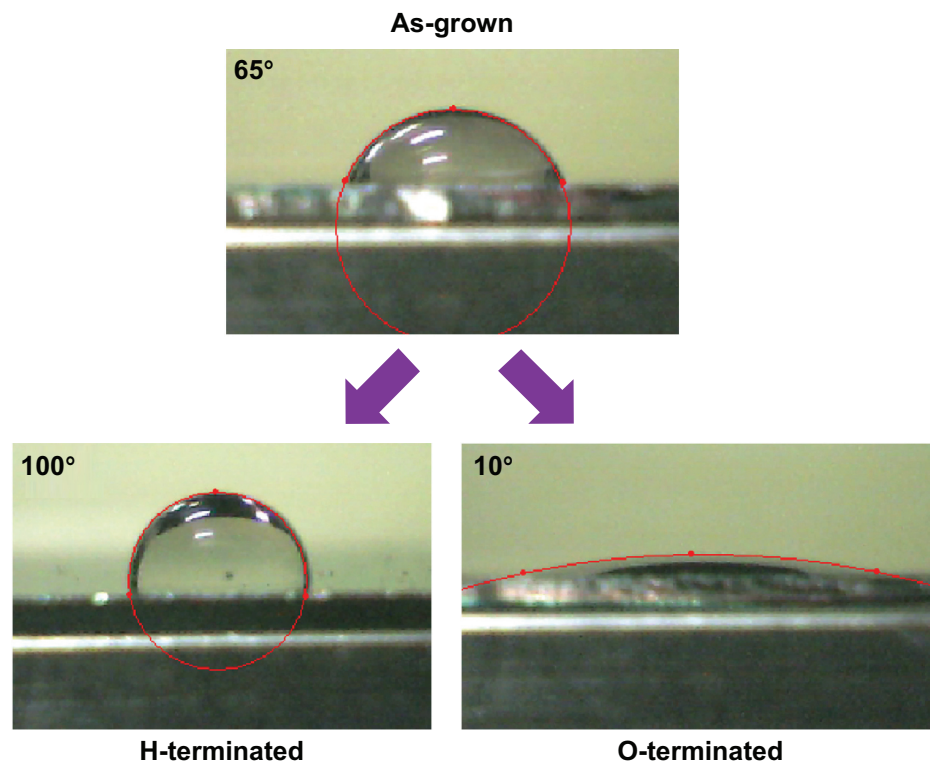
**Figure 2** Wetting properties of as-grown and treated diamond films in hydrogen plasma (H-terminated) or oxygen plasma (O-terminated).

because surface roughness of the diamond film that was used was much greater (approximately 18 nm).

By using modeling software for the optical properties of thin films (Film Wizard™; Scientific Computing International, Carlsbad, CA, USA), the thickness of the diamond film was evaluated from the interference fringes in the reflectance spectra that were measured in the visible and near infrared region. The calculated thickness for the diamond deposited on the Si smooth side was 420 nm and on the Si rough side about 250 nm. Although the deposition conditions were the same for both sides of the Si substrate (smooth and rough), lower diamond film thickness was obtained on the rough side, probably because the micrometer-scale substrate roughness probably caused slower closure of the diamond film.

## Cell number and proliferation

The cell numbers on the NCD surfaces and on the control microscopic glass were evaluated at 24 hours and 72 hours after seeding (Figure 3). At the 24-hour time point, there were no statistical differences in cell numbers among the H-terminated NCD, O-terminated NCD, and the control microscopic glass coverslips. The resulting densities (mean ± SD) at 24 hours after seeding were as follows: $13,792\pm3,492$ cells/cm$^2$ for H-terminated NCD films;

$14,461\pm8,132$ cells/cm$^2$ for O-terminated NCD films; and $16,249\pm6,061$ cells/cm$^2$ for the glass control. Since the seeding density was 10,000 cells/cm$^2$ and all of the samples revealed higher cell numbers, the cells at the 24-hour time point had probably already started to divide. However, the cells were not fully spread at this time.

On day 3 (72 hours after seeding), the cell numbers for the O-terminated NCD films were significantly higher than the cell numbers for the H-terminated NCD films. The glass control cell numbers on day 3 were lower than the numbers for either of the NCD surfaces.

## Differentiation of the cells

The Saos-2 cells were seeded at a density of 25,000 cells/cm$^2$ and were cultivated in the growth medium until confluence. After reaching confluence, the cell layers were stimulated to produce ECM by the addition of AA to the medium (to result in a concentration of 50 μg/mL) and were cultivated for 14 more days. Thereafter, the production of the ECM was evaluated in the resulting cell layers by monitoring several markers: production of type I collagen; activity of alkaline phosphatase (an enzyme participating in matrix mineralization); and deposition of calcium.

Figure 4 shows the appearance of the cell layers after 14 days of cultivation in the medium with the addition of AA.
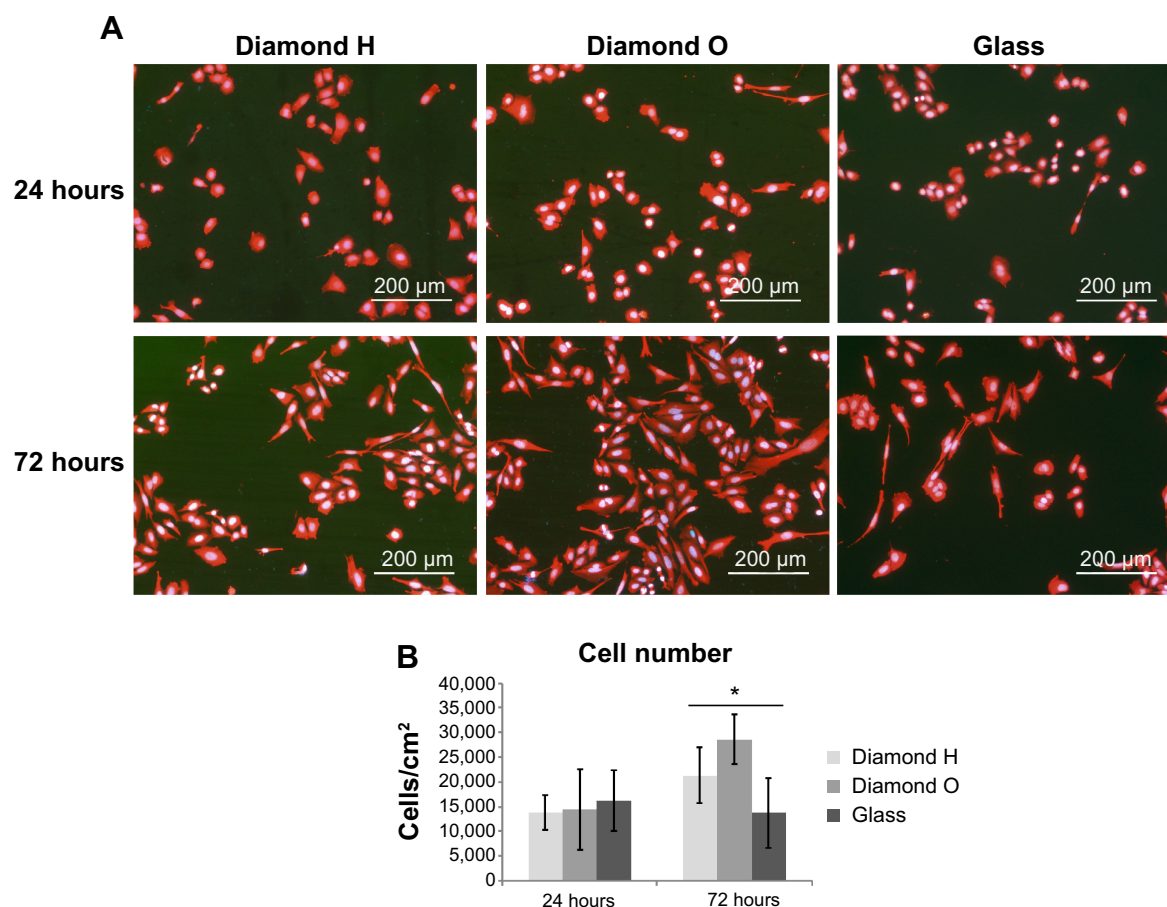
**Figure 3** Cell adhesion and growth on NCD films.
**Notes:** Fluorescence microscopy images showing the morphology of Saos-2 cells at 24 hours and 72 hours after seeding on H-terminated NCD films, on O-terminated NCD films, and on glass; Texas Red and Hoechst staining, fluorescence microscopy (Olympus IX 51) (**A**). Graph showing the number of Saos-2 cells at 24 hours and 72 hours after seeding on H-terminated NCD films, on O-terminated NCD films, and on glass; seeding density was $10 \times 10^3$ cells/cm$^2$. The data from ten images in each group are expressed as the mean ± SD. *Statistically significant at $P \leq 0.05$ (**B**).
**Abbreviations:** NCD, nanocrystalline diamond; SD, standard deviation.

LIVE/DEAD staining of the cell layers (Figure 4A) revealed no noticeable differences between the examined surfaces. A significant proportion of the cells were living (green staining), but there were also dead cells present (red staining). Immunofluorescence staining of type I collagen in the cell layers demonstrated the presence of collagen fibers in the produced ECM (Figure 4B). The cells were also stained because synthesized type I collagen was localized intracellularly.

## Characterization of collagen deposition

Together, the lack of centrosymmetry and the high crystallinity in the assembled type I collagen fibers resulted in significant levels of SHG,[28] which enabled SHG imaging of the collagen fibers. Fibrillar protein deposition was detectable by SHG imaging in the cell layers on both the H-terminated and O-terminated NCD films, and also in the control cell layers on microscopic glass (Figure 5). Because of significant

bleed-through of autofluorescence of the cells into the SHG channel, we also acquired control images with cell autofluorescence only.

We quantified the area of the SHG signal of mature extracellular collagen in the images. The percentage of the SHG signal area was lower on the H-terminated NCD films than on the O-terminated NCD films or on the microscopic glass. However, the difference was not statistically significant ($P=0.055$) when analyzed by ANOVA.

The overall collagen production in the cell layers was also quantified. The pepsin-soluble collagen content in the ECM was determined by Sirius red stain binding. The collagen production in the cell layers on the H-terminated NCD films was significantly lower than the collagen production on both the O-terminated NCD films and the polystyrene controls (Figure 6A). This difference was not caused by a different number of cells; the cell numbers on all surfaces were similar, as proven by the total DNA content (Figure
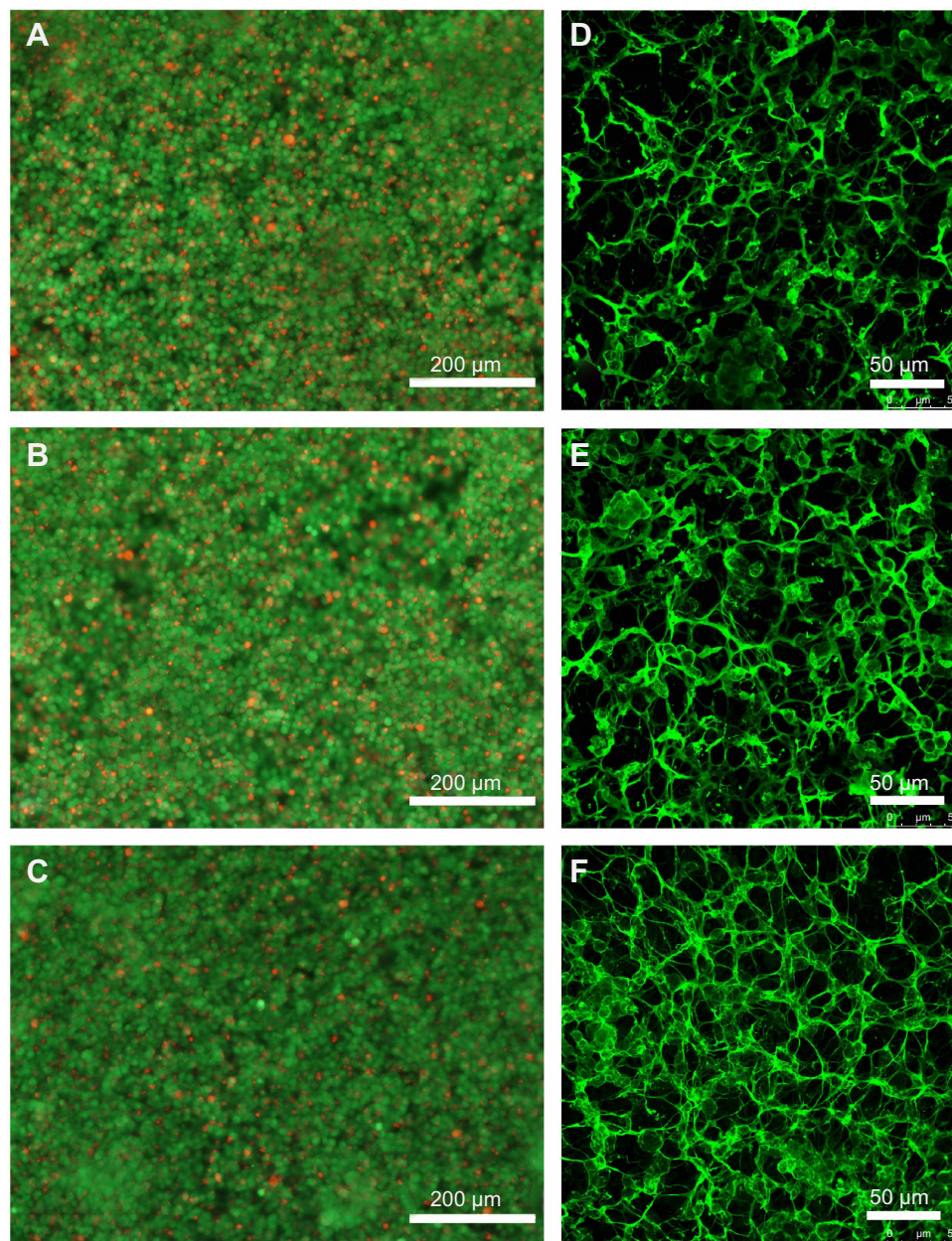
**Figure 4** Appearance of the cell layers on NCD films.
**Notes:** LIVE/DEAD staining (**A–C**) and immunofluorescence staining of type I collagen (**D–F**) in Saos-2 cells after 2-week culture in the medium with added AA on H-terminated NCD films (**A** and **D**); on O-terminated NCD films (**B** and **E**); and on glass (**C** and **F**). Seeding density was $25 \times 10^3$ cells/cm$^2$; differentiation occurred after confluence. Fluorescence microscopy (Olympus IX 51) (**A–C**). Confocal microscopy (Leica TCS SPE), maximum projection (**D–F**).
**Abbreviations:** NCD, nanocrystalline diamond; AA, ascorbic acid.

7B). The amount of deposited type I collagen on the O-terminated NCD films was comparable to the amount on the polystyrene controls.

## ALP activity and mineralization of ECM

After being normalized per substrate area, the ALP activity of the cell layers was significantly higher on the O-terminated NCD surfaces than on the H-terminated NCD films (Figure 6B). The cells that were grown on the polystyrene controls exhibited even lower ALP activity. Calcium deposition as a marker of ECM mineralization was determined in cell layers cultivated in both the standard growth medium and the medium with the addition of AA. The calcium deposition normalized per substrate area differed under different cultivation conditions and also on different surfaces. The calcium content of cell layers grown on O-terminated NCD films in both the standard medium and the medium with added AA ($14.34\pm1.05$ µg/cm$^2$ and $13.76\pm1.17$ µg/cm$^2$, respectively)
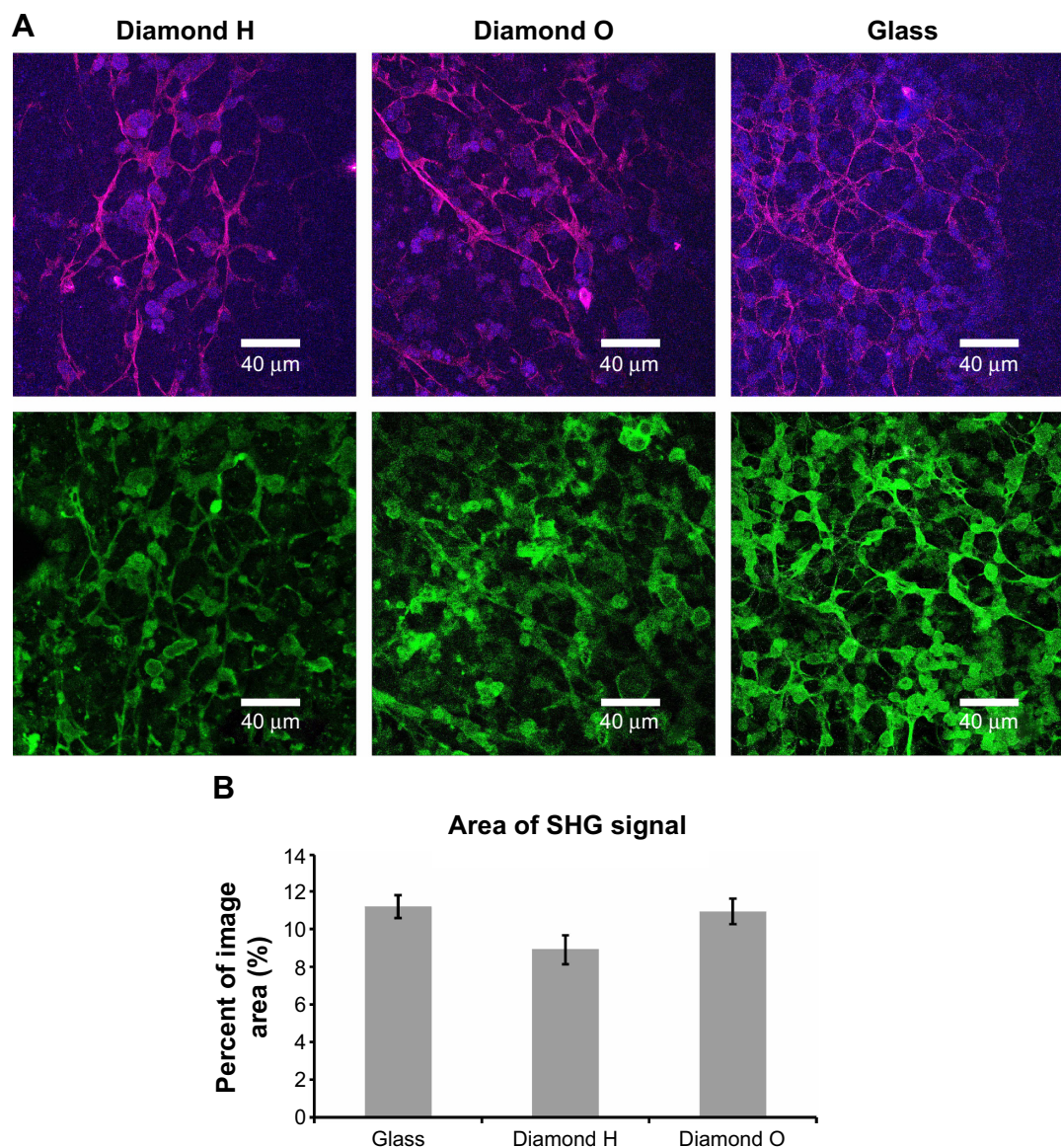
**Figure 5** SHG imaging showing collagen fibers in the cell layers on NCD films.
**Notes:** SHG signal (magenta), type I collagen immunofluorescence staining (green), and cell autofluorescence (blue) of Saos-2 cells after 2-week culture in the medium with added AA on H-terminated NCD films, on O-terminated NCD films, and on glass. The bar represents 40 µm (**A**). The area producing an SHG signal and green fluorescence was assessed by image analysis of 25 images in each group. Seeding density was $25 \times 10^3$ cells/cm$^2$; differentiation occurred after confluence. Confocal microscopy (Leica SP2). Data are expressed as the mean ± SD (**B**).
**Abbreviations:** SHG, second harmonic generation; NCD, nanocrystalline diamond; AA, ascorbic acid; SD, standard deviation.

was significantly higher than the calcium content on both of the H-terminated NCD films and the polystyrene controls (Figure 7A). The mineralization on the H-terminated NCD films was low ($6.06 \pm 0.66$ µg/cm$^2$), and with the added AA it was even lower ($3.61 \pm 0.66$ µg/cm$^2$). On the polystyrene controls, the calcium content also decreased with the addition of AA. The total DNA content, an indicator of the cell number, was comparable among the cell layers grown on all the substrates used in the experiments and also under both growth and differentiation conditions (Figure 7B).

## Expression of osteoblast differentiation markers

The expression of osteoblast differentiation markers (type I collagen, ALP, and osteocalcin) was determined by reverse transcription and real-time PCR on day 14 of cultivation of postconfluent cell layers in the normal growth medium and in the medium with added AA (Figure 8). With the addition of AA, ALP expression increased on both NCD surfaces. Although to a lesser extent, ALP expression increased significantly also on the polystyrene dishes. The expression of type I collagen also increased with the addition of AA.
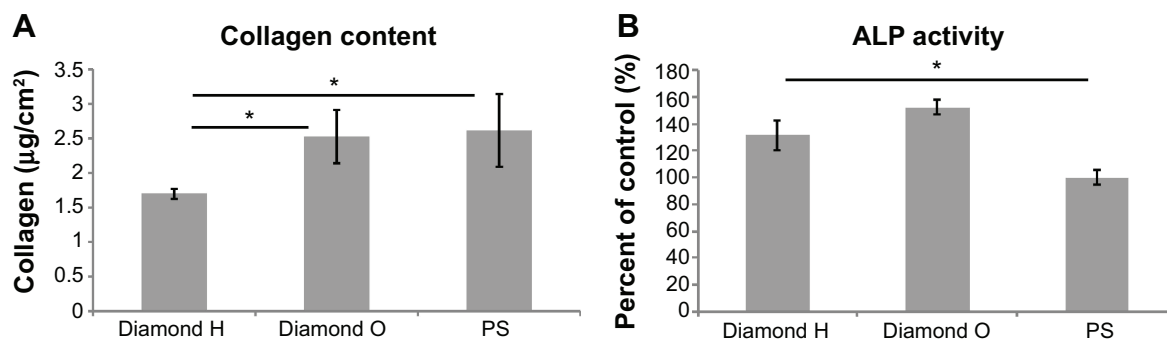
**Figure 6** Collagen content and ALP activity in the cell layers on NCD films.
**Notes:** (**A**, **B**) Saos-2 cells after 2-week culture in the medium with added AA on H-terminated NCD films (Diamond H), on O-terminated NCD films (Diamond O), and on PS. Seeding density was $25 \times 10^3$ cells/cm$^2$, differentiation after confluence. The collagen content and ALP activity were normalized by the substrate area; the ALP activity was expressed as a percentage of the control (PS=100%). Data are expressed as the mean ± SD. *Statistically significant at $P \leq 0.05$.
**Abbreviations:** PS, cell culture polystyrene dishes; ALP, alkaline phosphatase; NCD, nanocrystalline diamond; AA, ascorbic acid; SD, standard deviation.

The increase was more prominent on both NCD surfaces than on the polystyrene dishes; however, the difference in type I collagen expression on cell culture polystyrene was still statistically significant. Osteocalcin expression did not change with the addition of AA on either of the surfaces that were tested. Cells grown in the medium with added AA on H-terminated and O-terminated NCD films did not differ significantly in the expression of any of the examined osteoblast differentiation markers. However, in the growth medium, the expression of ALP and type I collagen was significantly lower on the O-terminated NCD films than on the other media.

The expression levels in Saos-2 cells grown on the H-terminated and O-terminated NCD films also did not differ significantly on days 1, 3, and 7 postconfluence (data not shown).

## Discussion

Until now, biological studies on NCD films with tuned wettability have been predominantly focused on osteoblast

adhesion and growth,[29] or on short-term osteogenic differentiation.[30,31] Some studies have also been focused on differentiation of neural stem cells, for which a hydrogenated NCD surface supports differentiation into neurons while an oxygenated NCD surface supports differentiation towards oligodendrocytes.[32,33] The process of osteoblast differentiation and ECM production may determine the osteoconductivity of the biomaterial.[10] We therefore tried to characterize the ability of osteoblast differentiation and of ECM deposition on the NCD films. The production and maturation of type I collagen was one of the markers that reflected cell differentiation and the quality of the deposited ECM.

The Saos-2 cell line is a human osteoblast-like cell line derived from osteosarcoma.[34] Another frequently used osteoblast cell line, MG-63,[35] phenotypically resembles immature osteoblasts; therefore, cells from that line are appropriate for studies of cell adhesion to biomaterials.[36] The phenotype of the Saos-2 cell is considered to have a mature osteoblast phenotype because it reproduces many of the primary human
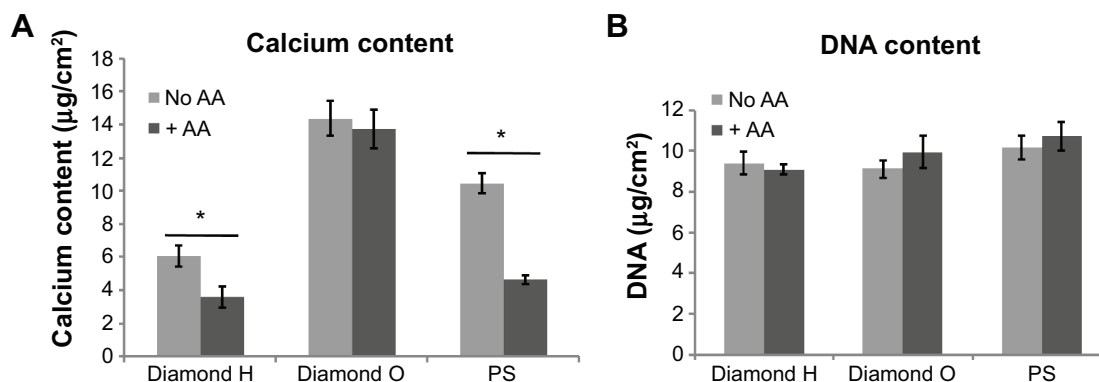


**Figure 7** Calcium deposition and DNA content in the cell layers on NCD films.
**Notes:** (**A**, **B**) Saos-2 cells after 2-week culture in the growth medium (No AA) or with added AA (+AA) on H-terminated NCD films (Diamond H), on O-terminated NCD films (Diamond O), and on PS. Seeding density was $25 \times 10^3$ cells/cm$^2$, differentiation occurred after confluence. The calcium content and DNA content were normalized by the substrate area. Data are expressed as the mean ± SD. *Statistical significance at $P \leq 0.05$.
**Abbreviations:** PS, cell culture polystyrene dishes; AA, ascorbic acid; NCD, nanocrystalline diamond; SD, standard deviation.
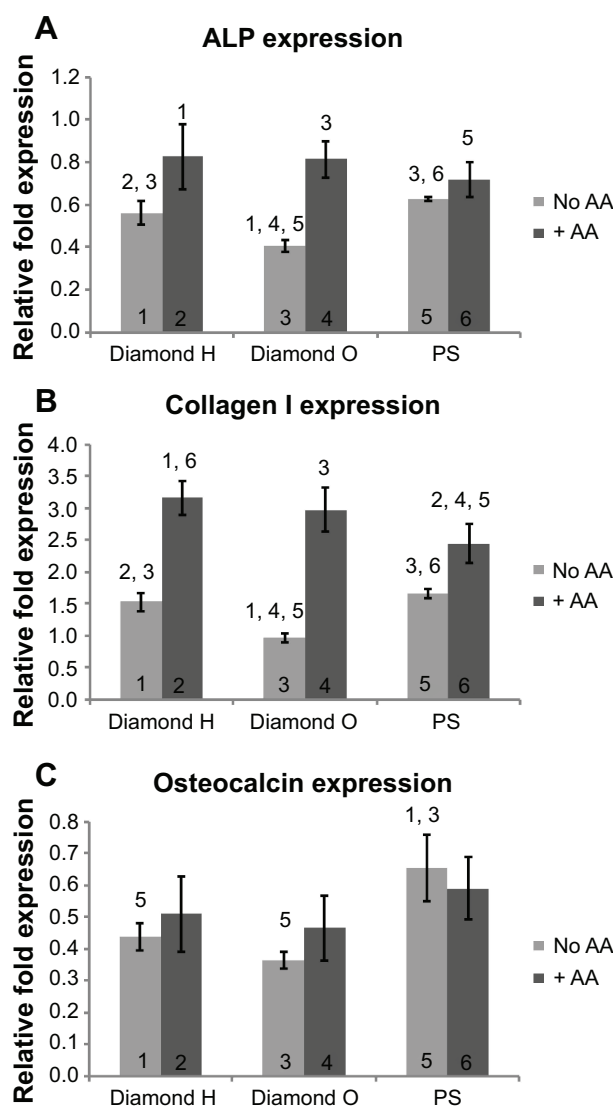
## A ALP expression



## B Collagen I expression



## C Osteocalcin expression



**Figure 8** Expression of the bone-specific genes.
**Notes:** (**A–C**) Gene expression of the osteogenic markers ALP, collagen I, and osteocalcin determined by real-time PCR in Saos-2 cells after 2-week culture in the growth medium (no AA) or with added AA (+ AA) on H-terminated NCD films (diamond H), on O-terminated NCD films (diamond O), and on PS. Seeding density was $25 \times 10^3$ cells/cm^{2}, differentiation occurred after confluence. The relative fold expression was related to the control cells grown on PS at day 0 of differentiation and was normalized by GAPDH expression. The numbers above the columns mark statistically significant ($P \leq 0.05$) difference compared to the group labelled with the same number at the base of the column.
**Abbreviations:** ALP, alkaline phosphatase; PS, cell culture polystyrene dishes; AA, ascorbic acid; collagen I, type I collagen; PCR, polymerase chain reaction; NCD, nanocrystalline diamond; GAPDH, glyceraldehyde 3-phosphate dehydrogenase.

osteoblast responses.[37] Saos-2 cells are also able to produce collagenous mineralized bone matrix containing type I and type V collagen and chondroitin sulfate proteoglycans.[38–40] Being from a cell line, Saos-2 cells are available for experiments in high numbers, and they are therefore ideal for studies of ECM deposition for which a hyperconfluent layer of cells is needed. In addition, the Saos-2 cell line is advantageous because of its phenotype stability during multiple passages.[41]

Saos-2 cells were stimulated to produce collagenous ECM with the addition of AA to the growth medium. Other commonly applied osteogenic additives, namely dexamethasone and β-glycerolphosphate, were shown to be toxic for Saos-2 cells (β-glycerolphosphate[42]) or to decrease collagen deposition (dexamethasone[43]). We also observed toxicity when β-glycerolphosphate was added to Saos-2 cells (data not shown); we therefore used only AA to stimulate ECM deposition.

The cell numbers on H-terminated and O-terminated NCD films were comparable after 24 hours, and cell division had already started. A previous study had shown that cells attached preferentially to the O-terminated stripes of NCD films; this effect was dependent on the presence of serum proteins in the cultivation medium.[29] An earlier paper had also reported a greater spreading area of osteoblasts on O-terminated NCD films 12 hours after seeding.[44]

In our experiments, cell attachment to H-terminated NCD films was probably slower, but the final cell number 24 hours after seeding did not differ significantly from the number of cells attached to the O-terminated NCD surface or to the microscopic glass. We observed earlier that the cell focal adhesions visualized by talin immunostaining were less prominent on H-terminated NCD films than on the other media. On O-terminated NCD films, the focal adhesions were more numerous and more apparent (Figure 9).[45] On the basis of these results, we hypothesize that there is weaker cell adhesion on H-terminated NCD films. Similar results were also obtained in earlier studies by other authors who observed either no focal adhesion plaques or less-developed focal adhesion plaques in cells cultured on hydrophobic surfaces, which were formed by coating glass with octadecylsilane, than on hydrophilic surfaces, which were represented by a clean glass substrate.[46] Moreover, measured by the movement and clustering of integrin receptors, the dynamics of the assembly of focal adhesion plaques was slower on hydrophobic surfaces.[47]

At 72 hours after seeding, the cell numbers on O-terminated NCD films were significantly higher than those on the H-terminated NCD films and on the microscopic glass. This difference suggests that the mitotic rate of the cells was higher on the O-terminated NCD films than on the other media. In subsequent experiments, a higher seeding density was used, and the cell layers were differentiated for 14 days after reaching confluence. The Saos-2 cells slowed down their cell cycle when confluent;[48] therefore, the resulting cell density was equal on all the examined surfaces (Figure 7).

The differences in cell adhesion and growth on H-terminated and O-terminated NCD films can be explained
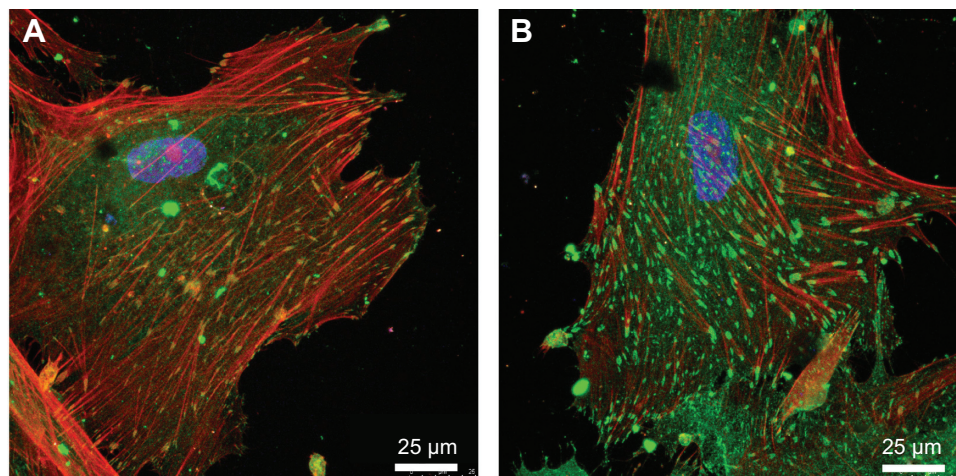
**Figure 9** The adhesion of primary human osteoblasts on H-terminated NCD films and O-terminated NCD films.
**Notes:** Primary human osteoblasts cultivated on H-terminated NCD films (**A**) and on O-terminated NCD films (**B**) for 7 days. The cells were stained for talin (green; immunofluorescence), actin (red; phalloidin/TRITC), and DNA (blue; DAPI). Similar results have been published.[45]
**Abbreviations:** NCD, nanocrystalline diamond; TRITC, tetramethylrhodamine; DAPI, 4′,6-diamidino-2-phenylindole.

by the differences in adsorption of cell adhesion-influencing molecules from the serum of the culture medium. These molecules comprise mainly albumin, vitronectin, and fibronectin, and their adsorption is influenced by the physical and chemical properties of the material surface, including the surface wettability. (For a review, see Bacakova et al[11].) In summary, H-terminated diamond surfaces typically consist of 1%–4% of oxygen because of inherent surface contamination from air; hence, they have hydrophobic surfaces.[49] Oxygen plasma-treated diamond typically exhibits an increased amount of C-O-C, C=O oxygen moieties; hence, O-terminated diamond surfaces become hydrophilic.[50,51] These results were similar to the observations from our XPS studies, not published here.

The selectivity of the adsorption of various proteins to surfaces that differ in wettability may result in a different composition and conformation of the protein layer adsorbed from FBS during seeding of the cells, and this influences cell adhesion to the material.[11] A study of the adsorption of protein to surfaces that differ in wettability showed that albumin had a stronger affinity for hydrophobic surfaces than for hydrophilic ones.[52] In addition, albumin is considered to be antiadhesive for cells.[53] The conformation of albumin and fibrinogen was less organized when they adsorbed onto a hydrophobic surface than when they adsorbed onto a hydrophilic surface.[52] In another study, the type IV collagen was adsorbed more to hydrophobic domains; however, the cells adhered preferentially to hydrophilic domains under the same conditions.[54] These data show that cell adhesion-mediating proteins can adsorb in a similar quantity or even in a higher quantity to hydrophobic surfaces, but the secondary structure of the adsorbed proteins is the key factor that

affects the adhesion and subsequent proliferation of the cells on the surface.[11]

Our results suggest that not only cell adhesion and growth, but also the process of ECM deposition by cells and the resulting composition of the ECM deposited on the material surface, are influenced by the wettability of the surface. Cell layers grown on wettable O-terminated NCD films revealed a higher total collagen content, higher ALP activity, and higher calcium deposition than did hydrophobic H-terminated NCD films. The underlying mechanism of material wettability is its surface free energy, which is directly proportional to the wettability. In accordance with this, human femur osteoblasts in cultures on NCD films terminated with H, O, or NH$_2$ showed a positive correlation of cell adhesion, growth, collagen production, and calcium deposition with the surface energy of the films.[44] Another study also described the relationship between differences in the quantity of collagen deposition and the wettability of the substrate. Specifically, calf chondrocytes in cultures on hydrophilic high density polyethylene deposited more collagen II than on the hydrophobic polymer.[55] We therefore hypothesize that O-terminated NCD films with wettability below 10° enhanced the deposition of bone-like ECM more than H-terminated surfaces did.

Type I collagen is the major component of organic bone ECM. In addition to their other functions, collagen fibers serve as a substrate for mineral deposition.[56] Collagen fiber formation, therefore, plays a crucial role in bone development, remodeling, and also in osseointegration of an implant. Our study showed that the total collagen content determined in cell layers was significantly higher on O-terminated NCD films than on H-terminated NCD films. The mature collagen

fibers were detected using the SHG technique on all of the examined surfaces, and no significant difference was found among those surfaces.

The expression of the three osteoblast differentiation marker genes on the level of mRNA was also determined by the real-time PCR method. The ALP enzyme bound in the cytoplasmic membrane plays an important role in bone calcification; it provides the increased phosphate concentration for hydroxyapatite crystallization.[57] Type I collagen is the major bone protein and, along with ALP, it is considered an early marker of osteoblast differentiation.[58] Some other studies regard type I collagen as an early marker and ALP as a middle marker of osteogenesis.[59] Osteocalcin (also known as bone gamma–carboxyglutamic acid-containing protein) is a noncollagenous calcium-binding bone protein referred to as a late osteogenic marker.[58] The expression of type I collagen, ALP, and osteocalcin genes under differentiation conditions with AA addition did not differ on NCD films with different wettability or on the control polystyrene dish. Under growth conditions, the expression of osteocalcin was significantly higher on the control polystyrene than on each of the NCD surfaces. The expression of type I collagen and ALP in the growth medium was lower on O-terminated NCD films than on the H-terminated NCD films and on the control polystyrene. This difference was small but statistically significant. This result could be explained by negative feedback generated by a higher amount of collagen, higher activity of ALP, and higher calcium deposition on O-terminated surfaces. Similarly, osteoblasts in cultures exposed to a mechanical load decreased the expression of ALP, osteocalcin, and collagen 1A1 genes, although immunocytochemistry revealed increased deposition of corresponding proteins.[60] Conversely, in transfected mouse myoblastic C2C12 cells producing MMP-10, which is an enzyme that cleaves matrix molecules, the levels of type 1 collagen, ALP, and osteocalcin mRNA were increased.[61] Another possible explanation for the lower expression of collagen I and ALP in cells on O-terminated surfaces is a higher proliferative activity (stimulation) of cells on these surfaces. The proliferation activity has often been reported to be inversely correlated to the cell differentiation, which includes the expression of collagen, ALP, and osteocalcin.[62] AA is a differentiation factor that attenuates cell proliferation[63] in the cell culture medium. The addition of AA probably masked the influence of the substrate's cell-growth properties on cell behavior; hence, on all tested surfaces, the differences in the expression of differentiation markers in cells equalized. It can also be supposed that the production of type I collagen and other differentiation markers is similar in cells on all tested

surfaces, but that O-terminated surfaces ensure the highest retention of these markers while the other substrates allow the release of these markers into the cell culture medium.

## Conclusion

O-terminated NCD films, which are hydrophilic, enhance the adhesion, growth, and osteogenic cell differentiation of Saos-2 cells. This effect is manifested by higher deposition and maturation of collagen I, higher activity of alkaline phosphatase, and higher matrix mineralization on O-terminated NCD films than on H-terminated NCD films, which are hydrophobic. Surprisingly, the expression of the genes for collagen I, ALP, and osteocalcin (ie, the levels of mRNA for these proteins) in cells on O-terminated surfaces was similar to or even lower than the expression in cells on H-terminated surfaces. This can be explained by a higher retention of mineralized matrix on O-terminated surfaces than on H-terminated surfaces. Thus, O-terminated NCD films are promising materials for coating bone implants in order to enhance their osseointegration and secondary stability.

## Acknowledgments

## Disclosure

The authors report no conflicts of interest in this work.

## References

1. Schrand AM, Huang H, Carlson C, et al. Are diamond nanoparticles cytotoxic? *J Phys Chem B.* 2007;111(1):2–7.
2. Bacakova L, Grausova L, Vandrovcova M, et al. Carbon nanoparticles as substrates for cell adhesion and growth. *Nanoparticles: New Research.* 2008;39–107.
3. Chen H, Shen J, Longhua G, Chen Y, Kim DH. Cellular response of RAW 264.7 to spray-coated multi-walled carbon nanotube films with various surfactants. *J Biomed Mater Res A.* 2011;96(2):413–421.

4. Song Z, Yang Z, Yang J, et al. Repair of abdominal wall defects in vitro and in vivo using VEGF sustained-release multi-walled carbon nanotubes (MWNT) composite scaffolds. *PloS One.* 2013;8(5):e64358.

5. Liu D, Yi C, Zhang D, Zhang J, Yang M. Inhibition of proliferation and differentiation of mesenchymal stem cells by carboxylated carbon nanotubes. *ACS Nano.* 2010;4(4):2185–2195.

6. Prajzler V, Varga M, Nekvindova P, Remes Z, Kromka A. Design and investigation of properties of nanocrystalline diamond optical planar waveguides. *Opt Express.* 2013;21(7):8417–8425.

7. Ondič L, Babchenko O, Varga M, Kromka A, Ctyroký J, Pelant I. Diamond photonic crystal slab: leaky modes and modified photoluminescence emission of surface-deposited quantum dots. *Sci Rep.* 2012;2:914.

8. Webster TJ, Hellenmeyer EL, Price RL. Increased osteoblast functions on theta + delta nanofiber alumina. *Biomaterials.* 2005;26(9):953–960.

9. Webster TJ, Ergun C, Doremus RH, Siegel RW, Bizios R. Enhanced functions of osteoblasts on nanophase ceramics. *Biomaterials.* 2000;21(17):1803–1810.

10. McMahon RE, Wang L, Skoracki R, Mathur AB. Development of nanomaterials for bone repair and regeneration. *J Biomed Materi Res B Appl Biomater.* 2013;101(2):387–397.

11. Bacakova L, Filova E, Parizek M, Ruml T, Svorcik V. Modulation of cell adhesion, proliferation and differentiation on materials designed for body implants. *Biotechnol Adv.* 2011;29(6):739–767.

12. Vagaská B1, Bacáková L, Filová E, Balík K. Osteogenic cells on bio-inspired materials for bone tissue engineering. *Physiological Res.* 2010;59(3):309–322.

13. Izak T, Novotná K, Kopová I, et al. Hydrogen-terminated diamond sensors for electrical monitoring of cells. *Key Eng Mater.* 2014;605: 577–580.

14. Grausova L, Kromka A, Bacakova L, Potocky S, Vanecek M, Lisa V. Bone and vascular endothelial cells in cultures on nanocrystalline diamond films. *Diam Relat Mater.* 2008;17(7):1405–1409.

15. Albrektsson T, Johansson C. Osteoinduction, osteoconduction and osseointegration. *Eur Spine J.* 2001;10(2):S96–S101.

16. Tye CE, Hunter GK, Goldberg HA. Identification of the type I collagen-binding domain of bone sialoprotein and characterization of the mechanism of interaction. *J Biol Chem.* 2005;280(14):13487–13492.

17. Embery G, Rees S, Hall R, Rose K, Waddington R, Shellis P. Calcium- and hydroxyapatite-binding properties of glucuronic acid-rich and iduronic acid-rich glycosaminoglycans and proteoglycans. *Eur J Oral Sc.* 1998;106 Suppl 1:267–273.

18. Mostaço-Guidolin LB, Ko AC, Wang F, et al. Collagen morphology and texture analysis: from statistics to classification. *Sci Rep.* 2013;3:2190.

19. Kromka A, Rezek B, Remes Z, et al. Formation of continuous nanocrystalline diamond layers on glass and silicon at low temperatures. *Chemical Vapor Deposition.* 2008;14(7–8):181–186.

20. Varga M, Izak T, Kromka A, Vesely M, Hruska K, Michalka M. Study of diamond film nucleation by ultrasonic seeding in different solutions. *Cent Eur J Phys.* 2012;10(1):218–224.

21. Williams OA, Douhéret O, Daenen M, Haenen K, Ōsawa E, Takahashi M. Enhanced diamond nucleation on monodispersed nanocrystalline diamond. *Chem Phys Lett.* 2007;445(4):255–258.

22. Kromka A, Babchenko O, Izak T, Hruska K, Rezek B. Linear antenna microwave plasma CVD deposition of diamond films over large areas. *Vacuum.* 2012;86(6):776–779.

23. Izak T, Babchenko O, Varga M, Potocky S, Kromka A. Low temperature diamond growth by linear antenna plasma CVD over large area. *Phys Status Solidi B.* 2012;249(12):2600–2603.

24. Varga M, Remes Z, Babchenko O, Kromka A. Optical study of defects in nano-diamond films grown in linear antenna microwave plasma CVD from H2/CH4/CO2 gas mixture. *Phys Status Solidi B.* 2012;249(12):2635–2639.

25. Ferrari AC, Robertson J. Interpretation of Raman spectra of disordered and amorphous carbon. *Phys Rev B.* 2000;61(20):14095–14107.

26. Kuzmany H, Pfeiffer R, Salk N, Günther B. The mystery of the 1,140 cm(−1) Raman line in nanocrystalline diamond films. *Carbon.* 2004;42(5–6):911–917.

27. Kromka A, Rezek B, Kalbacova M, et al. Diamond seeding and growth of hierarchically structured films for tissue engineering. *Adv Eng Mater.* 2009;11(7):B71–B76.

28. Campagnola PJ, Loew LM. Second-harmonic imaging microscopy for visualizing biomolecular arrays in cells, tissues and organisms. *Nat Biotechnol.* 2003;21(11):1356–1360.

29. Rezek B, Michalíková L, Ukraintsev E, Kromka A, Kalbacova M. Micro-pattern guided adhesion of osteoblasts on diamond surfaces. *Sensors.* 2009;9(5):3549–3562.

30. Grausova L, Bacakova L, Kromka A, et al. Nanodiamond as promising material for bone tissue engineering. *J Nanosci Nanotechnol.* 2009;9(6):3524–3534.

31. Kopecek M, Bacakova L, Vacik J, et al. Improved adhesion, growth and maturation of human bone-derived cells on nanocrystalline diamond films. *Phys Status Solidi (A).* 2008;205(9):2146–2153.

32. Chen YC, Lee DC, Hsiao CY, et al. The effect of ultra-nanocrystalline diamond films on the proliferation and differentiation of neural stem cells. *Biomaterials.* 2009;30(20):3428–3435.

33. Chen YC, Lee DC, Tsai TY, et al. Induction and regulation of differentiation in neural stem cells on ultra-nanocrystalline diamond films. *Biomaterials.* 2010;31(21):5575–5587.

34. Rodan SB, Imai Y, Thiede MA, et al. Characterization of a human osteosarcoma cell line (Saos-2) with osteoblastic properties. *Cancer Res.* 1987;47(18):4961–4966.

35. Billiau A, Edy VG, Heremans H, et al. Human interferon: mass production in a newly established cell line, MG-63. *Antimicrob Agents Chemother.* 1977;12(1):11–15.

36. Czekanska EM, Stoddart MJ, Ralphs JR, Richards RG, Hayes JS. A phenotypic comparison of osteoblast cell lines versus human primary osteoblasts for biomaterials testing. *J Biomed Mater Res A.* 2014; 102(8):2636–2643.

37. Saldaña L, Bensiamar F, Boré A, Vilaboa N. In search of representative models of human bone-forming cells for cytocompatibility studies. *Acta Biomater.* 2011;7(12):4210–4221.

38. McQuillan DJ, Richardson MD, Bateman JF. Matrix deposition by a calcifying human osteogenic sarcoma cell line (SAOS-2). *Bone.* 1995;16(4):415–426.

39. Saino E, Grandi S, Quartarone E, et al. In vitro calcified matrix deposition by human osteoblasts onto a zinc-containing bioactive glass. *Eur Cell Mater.* 2011;21:59–72; discussion 72.

40. Fernandes RJ, Harkey MA, Weis M, Askew JW, Eyre DR. The post-translational phenotype of collagen synthesized by SAOS-2 osteosarcoma cells. *Bone.* 2007;40(5):1343–1351.

41. Hausser HJ, Brenner RE. Phenotypic instability of Saos-2 cells in long-term culture. *Biochem Biophys Res Commun.* 2005;333(1):216–222.

42. Czekanska EM, Stoddart MJ, Richards RG, Hayes JS. In search of an osteoblast cell model for in vitro research. *Eur Cell Mater.* 2012;24:1–17.

43. Delaine-Smith RM, MacNeil S, Reilly GC. Matrix production and collagen structure are enhanced in two types of osteogenic progenitor cells by a simple fluid shear stress stimulus. *Eur Cell Mater.* 2012;24: 162–174.

44. Yang L, Li Y, Sheldon BW, Webster TJ. Altering surface energy of nanocrystalline diamond to control osteoblast responses. *J Mater Chem.* 2012;22(1):205–214.

45. Bacakova L, Kopova I, Stankova L, et al. Bone cells in cultures on nanocarbon-based materials for potential bone tissue engineering: A review. *Physica Status Solidi (A).* 2014;211(12):2688–2702.

46. Altankov G, Grinnell F, Groth T. Studies on the biocompatibility of materials: fibroblast reorganization of substratum-bound fibronectin on surfaces varying in wettability. *J Biomed Mater Res.* 1996;30(3):385–391.

47. Zlatanov I, Groth T, Lendlein A, Altankov G. Dynamics of beta-1-integrins in living fibroblasts – effect of substratum wettability. *Biophys J.* 2005;89(5):3555–3562.

48. Pautke C, Schieker M, Tischer T, et al. Characterization of osteosarcoma cell lines MG-63, Saos-2 and U-2 OS in comparison to human osteoblasts. *Anticancer Res.* 2004;24(6):3743–3748.

49. Haensel T, Uhlig J, Koch RJ, et al. Influence of hydrogen on nanocrystalline diamond surfaces investigated with HREELS and XPS. *Phys Status Solidi (A).* 2009;206(9):2022–2027.

50. Shirafuji J, Sakamoto Y, Furukawa A, Shigeta H, Sugino T. X-ray photoelectron spectroscopy analysis of plasma-treated surfaces of diamond films. *Diam Relat Mater.* 1995;4(7):984–988.

51. Klauser F, Ghodbane S, Boukherroub R, et al. Comparison of different oxidation techniques on single-crystal and nanocrystalline diamond surfaces. *Diam Relat Mater.* 2010;19(5):474–478.

52. Roach P, Farrar D, Perry CC. Interpretation of protein adsorption: surface-induced conformational changes. *J Am Chem Soc.* 2005;127(22): 8168–8173.

53. Wang DA, Ji J, Sun YH, Shen JC, Feng LX, Elisseeff JH. In situ immobilization of proteins and RGD peptide on polyurethane surfaces via poly(ethylene oxide) coupling polymers for human endothelial cell growth. *Biomacromolecules.* 2002;3(6):1286–1295.

54. Filová E, Bullett N, Bačaková L, et al. Regionally-selective cell colonization of micropatterned surfaces prepared plasma polymerization of acrylic acid and 1, 7-octadiene. *Physiol Res.* 2009;58(5):669–684.

55. LiVecchi AB, Tombes RM, LaBerge M. In vitro chondrocyte collagen deposition within porous HDPE: substrate microstructure and wettability effects. *J Biomed Mater Res.* 1994;28(8):839–850.

56. Boskey AL, Roy R. Cell culture systems for studies of bone and tooth mineralization. *Chem Rev.* 2008;108(11):4716–4733.

57. Anderson HC. Mechanism of mineral formation in bone. *Laboratory Investigation.* 1989;60(3):320–330.

58. zur Nieden NI, Kempka G, Ahr HJ. In vitro differentiation of embryonic stem cells into mineralized osteoblasts. *Differentiation.* 2003;71(1):18–27.

59. Gong Z, Wezeman FH. Inhibitory effect of alcohol on osteogenic differentiation in human bone marrow-derived mesenchymal stem cells. *Alcohol Clin Exp Res.* 2004;28(3):468–479.

60. Struewer J, Roessler PP, Schuettler KF, et al. Influence of cyclical mechanical loading on osteogenic markers in an osteoblast-fibroblast co-culture in vitro: tendon-to-bone interface in anterior cruciate ligament reconstruction. *Int Orthop.* 2014;38(5):1083–1089.

61. Mao L, Yano M, Kawao N, Tamura Y, Okada K, Kaji H. Role of matrix metalloproteinase-10 in the BMP-2 inducing osteoblastic differentiation. *Endocrine J.* 2013;60(12):1309–1319.

62. Marzia M, Sims NA, Voit S, et al. Decreased c-Src expression enhances osteoblast differentiation and bone formation. *J Cell Biol.* 2000;151(2):311–320.

63. Takamizawa S, Maehata Y, Imai K, Senoo H, Sato S, Hata R. Effects of ascorbic acid and ascorbic acid 2-phosphate, a long-acting vitamin C derivative, on the proliferation and differentiation of human osteoblast-like cells. *Cell Biol Int.* 2004;28(4):255–265.

64. Frank O, Heim M, Jakob M, et al. Real-time quantitative RT-PCR analysis of human bone marrow stromal cells during osteogenic differentiation in vitro. *J Cell Biochem.* 2002;85(4):737–746.

65. Zhang L, Ren X, Alt E, et al. Chemoprevention of colorectal cancer by targeting APC-deficient cells for apoptosis. *Nature.* 2010;464(7291):1058–1061.